The Hypoxia-regulated Ectonucleotidase CD73 is a Host Determinant of HIV Latency

Hannah S. Sperber[1,2,3,6], Kyle A. Raymond[1,3], Mohamed S. Bouzidi[1,3], Tongcui Ma[3,4], Silvana Valdebenito[5], Eliseo Eugenin[5], Nadia R. Roan[3,4], Roland Schwarzer[6], Satish K. Pillai[1,3*]

1. Vitalant Research Institute, San Francisco, California, United States of America

2. Free University of Berlin, Institute of Biochemistry, Berlin, Germany

3. University of California, San Francisco, California, United States of America

4. Gladstone Institutes, San Francisco, CA, United States of America

5. The University of Texas Medical Branch, Galveston, TX, United States of America

6. University Hospital Essen, Institute for Translational HIV Research, Essen, Germany

*Correspondence: satish.pillai@ucsf.edu

SUMMARY

Deciphering the mechanisms underlying viral persistence is critical to achieving a cure for HIV infection. We uncovered molecular signatures of HIV latently-infected CD4+ T cells, identifying the adenosine-producing ectonucleotidase CD73 as a key marker of latent infection. Hypoxic conditioning, reflective of tissue microenvironments, increased the frequency of CD73+ CD4+ T cells and promoted HIV latency. Transcriptomic profiles of CD73+ CD4+ T cells indicated expression phenotypes favoring viral persistence, immune evasion, and cell survival. Further, we demonstrate that CD73+ CD4+ T cells harbor a functional HIV reservoir and are capable of reinitiating productive infection *in vitro*. Moreover, blocking of the A2A receptor facilitates HIV reactivation *in vitro*, linking adenosine signaling to viral quiescence. Finally, tissue imaging of lymph nodes from HIV-infected individuals on antiretroviral therapy reveal spatial association between CD73 expression and HIV persistence *in vivo*. Our findings warrant exploration of the hypoxia-CD73-adenosine axis in curative strategies to promote viral eradication.

KEYWORDS

HIV, persistence, latency, reservoir, eradication, CD73, CD39, IL8, adenosine, hypoxia, lymphoid tissues, HIV cure.

INTRODUCTION

In recent decades, remarkable scientific and biomedical advances have turned the tides in the ongoing fight against the global human immunodeficiency virus (HIV) epidemic. However, current therapeutic regimens fail to completely eradicate HIV due to the persistence of latently-infected cells[1]. These viral reservoirs are established very early during infection, remain invisible to the host's immune system, and persevere for decades despite effective antiretroviral therapy (ART)[2–4]. Although latently-infected cells are extremely rare[5–7], they are able to reinvigorate spreading infection rapidly, and people living with HIV (PLWH) almost inevitably experience viral rebound within weeks of a treatment interruption[2,8].

The identification of reliable biomarkers or unique gene expression patterns in HIV latently-infected cells are key goals of current HIV research efforts. Such factors could contribute to the development of a cure by: 1) refining and broadening our understanding of HIV latency mechanisms and the biology of viral persistence, 2) enabling accurate quantification of viral reservoirs to assess viral burden and efficacy of therapeutic interventions, and 3) providing potential therapeutic targets to specifically eliminate viral sanctuaries. However, the heterogenous and dynamic nature of the viral reservoir greatly complicates this endeavor[9].

Viral reservoirs are found in a variety of anatomical sites and cell types. Infected CD4+ T cells arguably constitute the most important HIV reservoir[10] and within this highly diverse cell lineage, the expression of several cellular factors is associated with increased levels of integrated proviral DNA[11]. This includes immune checkpoint molecules such as programmed cell death protein 1 (PD1), cytotoxic T-lymphocyte-associated protein 4 (CTLA-4), lymphocyte-activation gene 3 (LAG-3), and TIGIT[9,12,13]. Moreover, expression levels of CD2 in CD4+ T cells were reported to identify HIV latently-infected cells[14], while CD20[15] and CD30[16] expressing CD4+ T cells were found to be specifically enriched for HIV RNA. In 2017, Descours et al.[17] proposed CD32a as viral reservoir marker and described an unprecedented

1000-fold enrichment in HIV DNA in CD32a+ cells as compared to CD32a- CD4+ T cells. However, this finding has been repeatedly challenged in subsequent studies and incited a controversial discussion[18–23].

In the present study, we sought to provide a better understanding of the phenotypic nature of latently infected CD4+ T cells and the mechanisms involved in the establishment and maintenance of HIV reservoirs. To this aim we utilized a dual-reporter HIV construct that enables isolation and purification of uninfected, productively-infected, and latently-infected cells[24,25] by flow cytometry. We then characterized each of these purified cell populations using systems approaches to obtain comprehensive gene and protein expression profiles of HIV latently-infected, primary CD4+ T cells. Our data reveal a novel mechanism of HIV latency establishment and maintenance, identifying the hypoxia-CD73-adenosine signaling axis as a key mechanism and potential target for therapeutic intervention and diagnostic evaluation.

RESULTS

Sorting of HIV_{DFII}-infected primary CD4+T cells enables isolation of latently-infected cells. In order to be able to characterize latent HIV reservoir cells we utilized a modified version of a single round, recombinant HIV dual-reporter virus called HIV Duo-Fluo II (HIV_{DFII}) (Figure S1A). To achieve sufficient infection frequencies, we first activated blood-derived primary CD4+T cells obtained from six healthy donors *in vitro* via αCD3/αCD28 bead stimulation and then spinoculated them with HIV_{DFII} (Figure S1B-D). Four days post infection (p.i.), productively- and latently-infected, as well as uninfected cells were purified by fluorescence activated cell sorting (FACS, Figure 1A). Expectedly[25], low frequencies of latently-infected cells were found for all donors, whereas uninfected and productively-infected cells could be rapidly collected by FACS in large numbers (Figure 1B and C). After testing the sorted samples for sufficient enrichment of the desired cell populations (Figure S1E), we subjected them, together with a panel of control specimens (untreated samples; unstimulated, infected cells; and stimulated cells without HIV_{DFII} infection) to downstream analysis using systems approaches (Figure 1A). All samples were characterized using mass cytometry by time of flight (CyTOF), measuring 40 surface proteins to provide immunophenotypic profiles at the single cell level. In parallel, we applied NanoString hybridization and fluorescence-based digital counting technology allowing for simultaneous detection of 770 mRNA and 30 protein targets.

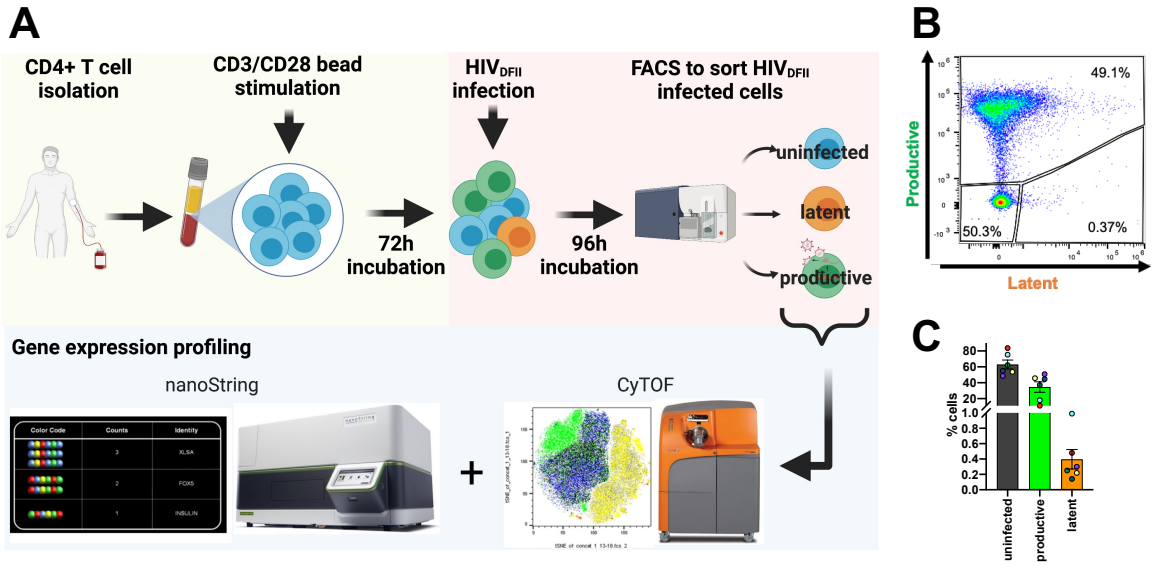

Figure 1: Isolation of latently-infected primary CD4+ T cells using the dual-reporter virus HIV_{DFII}. (A) Experimental workflow: Blood-derived primary CD4+ T cells were isolated from six healthy donors and stimulated *in vitro* with αCD3/αCD28 beads for three days. Cells were then infected with HIV_{DFII} and subjected to FACS 4 days post infection. (B) Representative gating for FACS of productively-infected, latently-infected, as well as uninfected CD4+ T cells. All samples were pre-gated for live, single cells. (C) Bar graph represents the distribution of infected cells of all six donors. Colored dots indicate individual donors. Error bars show standard error of the mean (SEM).

Latently-infected cells are phenotypically diverse and include T-regs and Tfh cells. First, to establish an in-depth analysis of the phenotypic features of latently-infected cells, we implemented CyTOF, simultaneously quantifying expression levels of 40 different proteins with single cell resolution. Our labeling panel comprised T cell lineage and differentiation markers, activation markers, homing receptors, and several proteins that were described previously in the context of HIV latency[9,26,27] (Table S1). We performed extensive high dimensional analysis and generated t-distributed stochastic neighbor embedding (tSNE) plots to visualize the data and assess specific T cell subsets and population phenotypes. Across all donors, we identified latent cells in various T cell compartments, including central memory (CD45RO+CD45RA-CCR7+CD27+), follicular helper (CD45RO+CD45RA-PD1+CXCR5+), regulatory (CD45RO+CD45RA-CD127-CD25+), and to a lesser extent naïve (CDRO-CDRA+CCR7+) T cells (Figure 2).

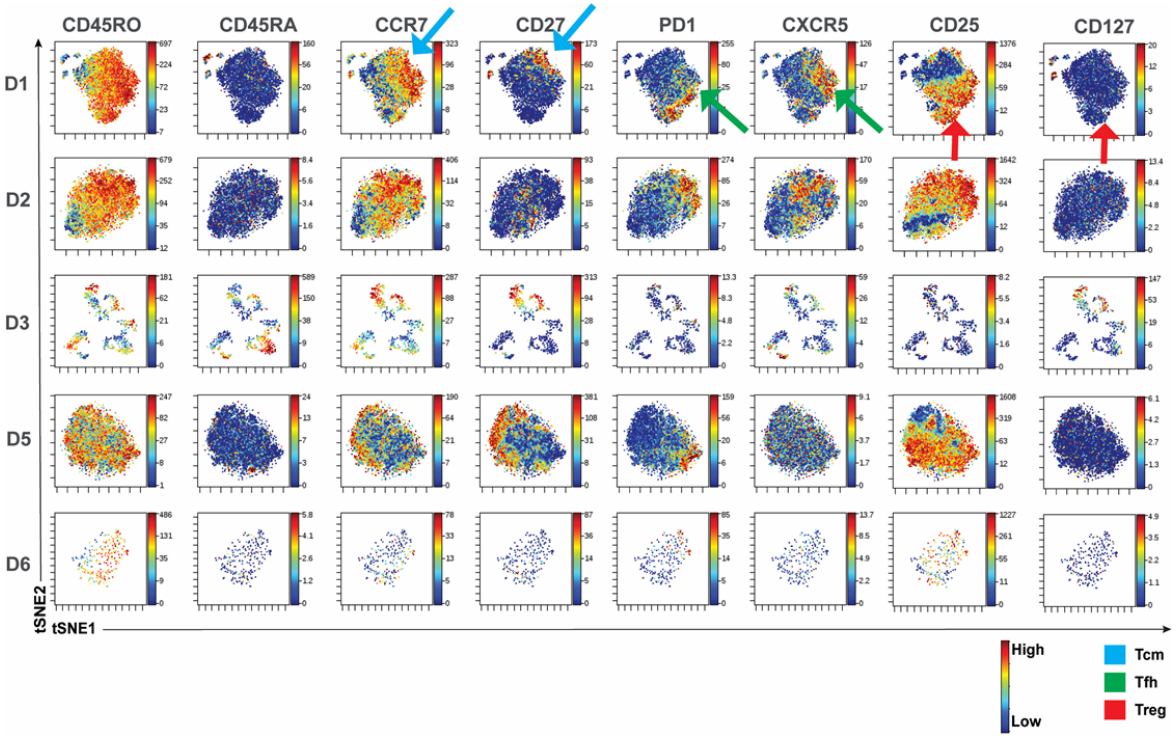

Figure 2: Multiple subsets of T cells, including T-regs, are represented among HIV-infected latent cells. Shown are tSNE plots of sorted latent cells from each of 6 donors (D1-D6), each analyzed within its own tSNE space. tSNEs are color-coded according to expression levels of the antigen listed at the top (with red corresponding to highest expression, and blue the lowest). We found that most cells exhibited a memory phenotype in that they expressed high levels of CD45RO and low levels of CD45RA (first two columns). Among the latent cells were those with phenotypic features of Tcm cells (CCR7+CD27+), Tfh cells (PD1+CXCR5), and Tregs (CD25+CD127-). Areas of the tSNE corresponding to these 3 subsets of cells are highlighted by the blue, green, and red arrows, respectively, for D1.

NanoString analysis reveals unique features of latently-infected cells that promote viral quiescence and cell survivorship. We next obtained high-dimensional NanoString data to comprehensively characterize gene and protein expression patterns of latent cells. Our initial analysis revealed that gene expression levels needed to be adjusted for donor effects that were revealed as confounding variables in an unsupervised clustering analysis (Figure 3A, see dendrogram). Importantly, we also found that expression patterns in uninfected and productively-infected cells within each donor clustered together while latently-

infected cells clustered separately, suggesting that latently-infected cells exhibited distinct expression signatures (Figure 3A, see dendrogram).

Subsequently, we examined changes in regulatory and signaling pathways in latent cells based on undirected and directed global significance scores (Figure 3B). The pathways 'Antigen Processing', 'Adhesion', 'Pathogen Defense', and 'Interleukins' exhibited the most significant changes. The upregulation of 'Interleukins' and 'Pathogen Defense' in latently-infected cells pointed towards intracellular signaling cascades that antagonize productive infection. In contrast, the suppression of 'Antigen Processing' in latent cells indicated the ability to evade host immunity, a pro-survival effect that could enforce viral persistence, and an observation in line with previous studies reporting that HIV actively modulates antigen presentation pathways[28,29].

Next, overall target expression in the sorted samples was assessed by differential gene expression analysis (DGE, Figure 3C). Comparison of uninfected and latently-infected cells revealed 16 differentially expressed targets (adjusted p-value < 0.1), two of which were identified at the protein level: HLA-DRA protein was downregulated, and NT5E (CD73) protein was upregulated in latent cells. DGE analysis between productively- and latently-infected cells resulted in 36 significant hits (adjusted p-value < 0.1). These included CD4 protein and CD73 protein. CD4 protein was significantly downregulated in productively-infected cells, indicating active viral replication, and CD73 protein was again upregulated in latent cells.

Overlapping both individual, differential expression analyses revealed 27 targets that were uniquely modulated in latent infection (p-value < 0.05, Figure 3D). Among these, CD73 was the only hit detected on the protein level (Table S2). The list further included three mRNAs encoding for transcription factors, 6 encoding for cytokines and 11 encoding for surface proteins. Among these, *NF-κBIA* (NF-κB Inhibitor Alpha) mRNA, which encodes a master inhibitor of the transcription factor

NF-κB[30], which in turn is a crucial transcription factor of HIV[31,32], was significantly upregulated in latent cells. In addition, *CASP1* mRNA was significantly downregulated in latently-infected cells. CASP1 (Caspase-1) is a key regulator of pyroptotic cell death, a highly inflammatory process that has been reported to be a major determinant of HIV pathogenesis and a potent driver of virus-dependent CD4+ T cell depletion[33].

The relationship between targets specific for latent infection was then investigated by utilizing the open-source software Cytoscape to generate a detailed protein-protein interaction network (Figure 3E). Interestingly, all genes were part of one protein interaction complex. The chemotactic factor IL8 (or CXCL8) was found to have the highest number of immediate connections (17 first neighbors), followed by the transcription factor STAT1 (15 first neighbors) and the cytokine CSF2 (15 first neighbors).

Three key members of the adenosinergic pathway, IL8, CD39, and CD73, are uniquely expressed in latent cells. In a more stringent attempt to pinpoint unique features of latent cells, we incorporated non-activated and non-virus-exposed samples in our NanoString analysis, thereby emulating the *in vivo* landscape in ART-suppressed individuals, where the majority of CD4+ T cells are likely in a resting state and have not encountered HIV. Here, expression signatures were clearly dominated by *in vitro* activation (Figure S2A and B). We therefore examined first if T cell activation is a determinant of HIV latency and investigated expression levels of established T cell surface markers CD45, CD45RO, and CD4 (Figure S2C) as well as panel-specific activation markers (Figure S2D and E). No significant associations were discovered between the expression levels of these markers and latent infection.

Next, latent cells were compared by DGE in a pair-wise fashion to all other samples. Of note, only a few differentially expressed genes were found in relation to HIV_{DFII}

exposed samples (Figure 3F) whereas differences were markedly broader towards virus naïve and non-activated samples. This demonstrated that distinct, albeit subtle expression patterns of latent cells can be found following our experimental approach. The pair-wise DGE analyses were then again overlaid to carve out genes uniquely changed in latently-infected cells (Figure 3G). We found three hits that were significantly changed with respect to all other comparators: IL8 mRNA, CD39 mRNA and CD73 protein (Figure 3H). Strikingly, this result comprised CD73 protein, a key hit from our previous analyses. In addition, the three genes are known to be mechanistically connected through the adenosine signaling pathway[34–38].

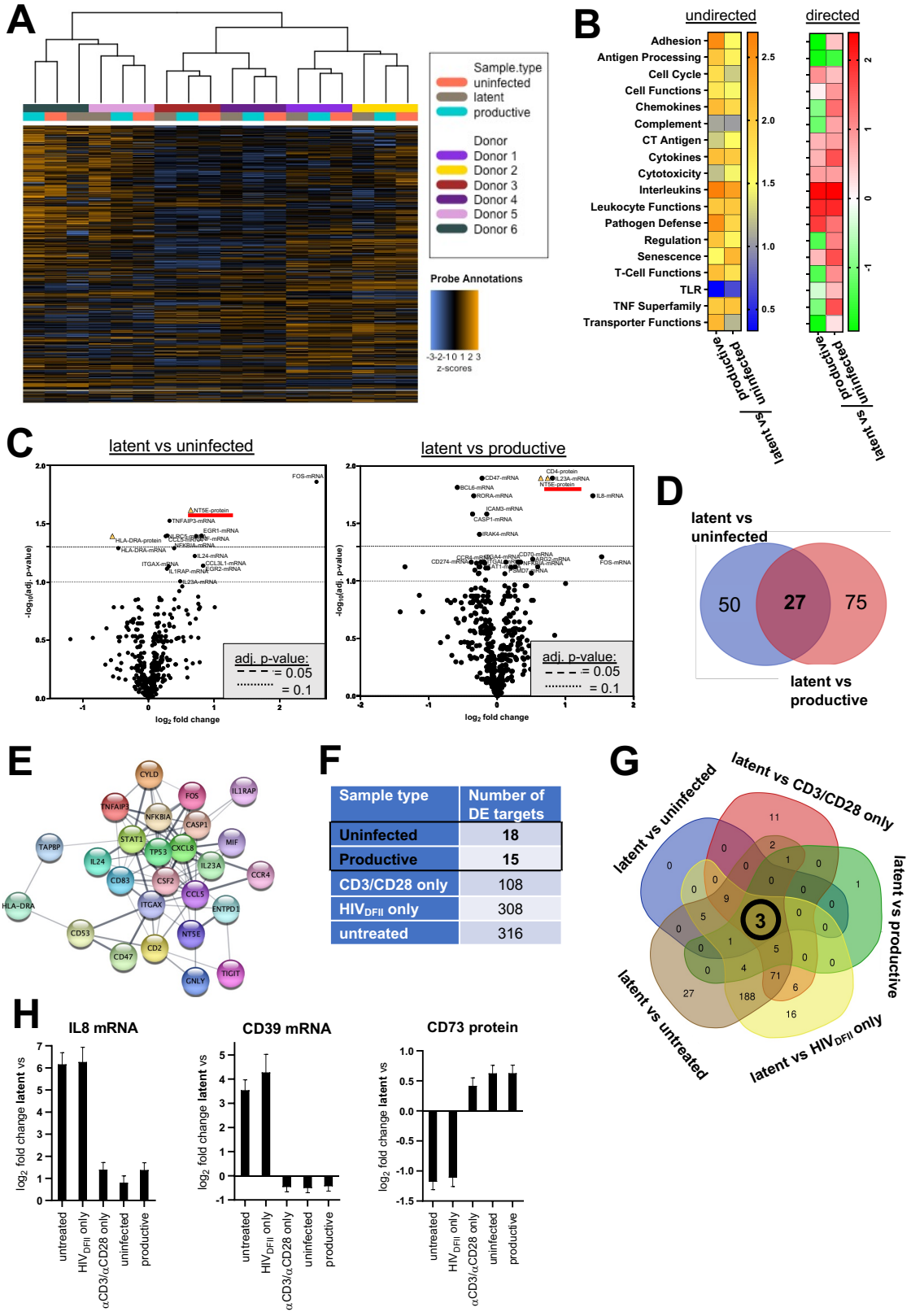
A
Sample.type
uninfected
latent
productive
Donor
Donor 1
Donor 2
Donor 3
Donor 4
Donor 5
Donor 6
Probe Annotations
-3 -2 -1 0 1 2 3
z-scores
B
undirected
directed
Adhesion
Antigen Processing
Cell Cycle
Cell Functions
Chemokines
Complement
CT Antigen
Cytokines
Cytotoxicity
Interleukins
Leukocyte Functions
Pathogen Defense
Regulation
Senescence
T-Cell Functions
TLR
TNF Superfamily
Transporter Functions
latent vs uninfected
latent vs productive
C
latent vs uninfected
latent vs productive
adj. p-value:
= 0.05
= 0.1
log2 fold change
-log10(adj. p-value)
D
latent vs uninfected
50
27
75
latent vs productive
E
CYLD
FOS
IL1RAP
TNFAIP3
NFKBIA
CASP1
STAT1
TAPBP
TP53
CXCL8
MIF
IL24
IL23A
CCR4
CD83
CSF2
CCL5
HLA-DRA
ITGAX
ENTPD1
CD53
NT5E
CD47
CD2
GNLY
TIGIT
F
Sample type
Number of DE targets
Uninfected
18
Productive
15
CD3/CD28 only
108
HIVDFII only
308
untreated
316
G
latent vs uninfected
latent vs CD3/CD28 only
latent vs productive
latent vs untreated
latent vs HIVDFII only
3
H
IL8 mRNA
CD39 mRNA
CD73 protein
log2 fold change latent vs
untreated
HIVDFII only
αCD3/αCD28 only
uninfected
productive

Figure 3: Latently-infected cells share signature features including distinct expression of IL8 mRNA, CD39 mRNA and CD73 protein. (A) Heatmap visualizing normalized gene expression data from unsupervised clustering analysis of virus-exposed, sorted samples. Each row shows normalized counts of a single probe (target) and each column represents an individual sample. Colored horizontal bars along the top identify assigned sample attributes (donor or sample type, see color legend). Hierarchical clustering was used to generate dendrograms. (B) Heatmaps showing undirected and directed global significance scores for signaling pathways based on differential gene expression analysis. (C) Volcano plots depict differential mRNA (circle) and protein (triangle) target expression between latent vs uninfected and latent vs productively-infected cells. Each data point represents one target. The $\log_2$ fold change is displayed on the x-axis and the $-\log_{10}$ of the adjusted (adj.) p-value (using the Benjamini-Hochberg method) on the y-axis. Horizontal lines indicate adj. p-value thresholds. The top 20 hits in each comparison are labeled. Hits were considered significant at an adj. p-value cutoff < 0.1. NT5E (CD73) is underlined in red. (D) Venn diagram illustrating overlapping hits from the DGE analyses 'latent vs uninfected' and 'latent vs productive' using a p-value cutoff $p < 0.05$. (E) A protein-protein interaction network of targets uniquely changed in latent cells was generated in Cytoscape 3.8.2. Applied was the STRING database for Homo sapiens with a confidence score of 0.4. Thickness of lines between nodes depicts confidence score with a thicker line representing a higher score. HLA-DRB3 was not recognized by the software and thus excluded from the interaction network. (F) Number of differentially expressed genes from pairwise-comparisons of latent cells to all other samples. Differential target expression between samples was compared with a p-value cutoff at < 0.05. (G) Venn diagram displaying the overlay of differential expression hits from comparisons of latently-infected cells with all other samples using a p-value cutoff at $p < 0.05$. (H) Bar graphs depict the $\log_2$ fold change of the indicated targets between latent cells and all other samples. Error bars show standard deviation (SD).

Hypoxia promotes CD73 expression and HIV latency in primary CD4+ T cells.

To better understand the relevance of CD73 in the context of HIV infection and particularly in the establishment of the latent reservoir, we next focused on the regulation of CD73 expression[39,40]. Importantly, at least one hypoxia-response element (HRE) has been previously identified in the CD73 promoter region[41] allowing for direct binding of hypoxia-inducible factors (HIFs). In this context, HIF-1α was demonstrated to control CD73 expression, with CD73 typically being upregulated under hypoxic conditions[42]. We therefore hypothesized that our discovery of CD73 upregulation in latent cells suggested that hypoxia may be the underlying cause of both increased CD73 expression and HIV latency.

We first confirmed our NanoString data using *in vitro* infection with HIV_{DFII} followed by immunofluorescence staining and flow cytometry, again observing a significant enrichment of CD73+ cells among latently-infected cells (Figure 4A and B). We then mimicked hypoxic conditions in our culture settings via administration of dimethyloxalylglycine (DMOG), followed by infection with HIV_{DFII} and flow cytometry (Figure 4C).

DMOG treatment drastically altered CD73 expression in CD4+ T cells and led to a 2.5-fold increase of CD73+ cells compared to mock treatment (Figure 4D and E). Notably, while CD73 expression was generally increased upon induction of hypoxic responses (compare Figure 4B and Figure S3A), we observed a pronounced enrichment of CD73+ cells specifically in the latent compartment with up to 60% of latent cells being CD73 positive (Figure S3A). This was also reflected in CD73 expression per cell measured by mean fluorescence intensities (MFIs), which showed an overall increased CD73 expression in latent cells in both, mock and DMOG treated samples (Figure S3B). Importantly, latent infection became significantly more abundant under hypoxic conditions with a 33.6% increase upon DMOG treatment, while the frequency of uninfected or productive cells did not change significantly between culture conditions (Figure 4F and G).

Lastly, we examined whether CD73+ cells were enriched for latent virus (Figure 4H). We measured a considerably higher rate of latently-infected cells in CD73+ compared to CD73- cells with an average 3-fold enrichment of latent infection within the CD73+ T cell compartment (Figure 4I). Considering the average frequency of CD73+ cells among CD4+ T cells (~10%, Figure 4E), these data suggest that approximately 25% of the overall, peripheral CD4+ T cell HIV reservoir may reside in CD73+ cells. Interestingly, the enrichment of latent cells in CD4+ CD73+ T cells did not significantly differ between mock- and DMOG-treated samples (Figure 4I), indicating that CD73+ cells may possess specific features that

favor the establishment and/or maintenance of latent infection that are not further modulated by the induction of hypoxic responses.

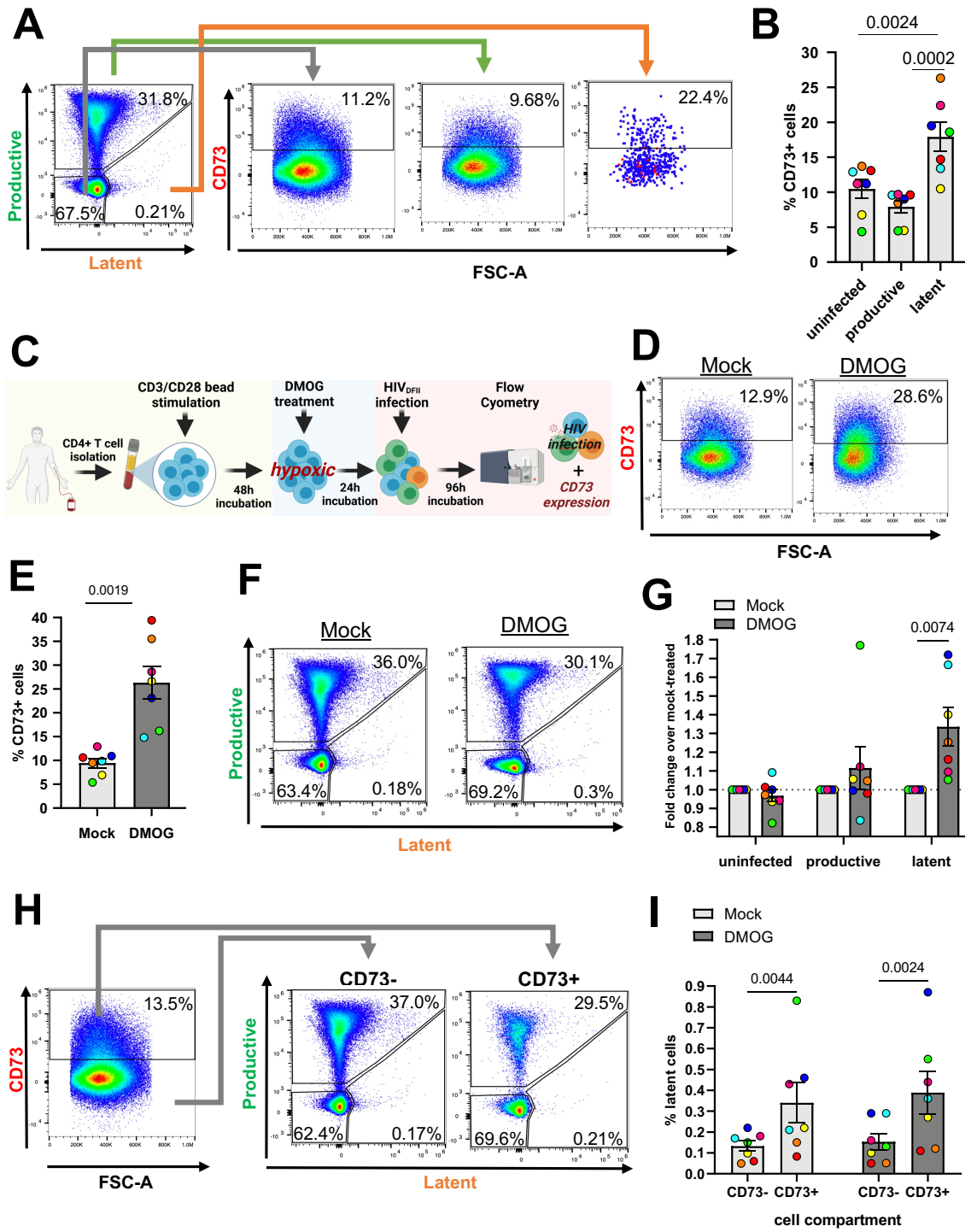

Figure 4: Hypoxic conditions increase the frequency of CD4+ CD73+ T cells and facilitate latent infection. (A) CD4+ T cells from healthy individuals were infected with HIV_{DFII} and analyzed by

immunofluorescence staining and flow cytometry. Scatter plots show the gating strategy to analyze CD73 expression in HIV_{DFII}-infected cells from a single, representative donor. (B) Shown is the frequency of CD73+ cells in the respective HIV_{DFII}-infected cell population summarized from 7 donors. P-values displayed above bars were generated by performing a one-way ANOVA with Tukey's multiple comparisons test. (C) Experimental workflow for HIV_{DFII} infection under hypoxic conditions. (D) Representative flow plots of CD73 immunofluorescence staining in mock or DMOG treated CD4+ T cells and (E) average frequency of CD73+ CD4+ T cells across 7 donors. The p-value was generated by performing a two-tailed paired t-test. (F) Representative flow plots, showing HIV_{DFII} infection profiles 4 days post HIV_{DFII} exposure upon mock or DMOG treatment. (G) The frequency of DMOG-treated, HIV_{DFII}-infected cells was normalized to the respective mock population within each donor to account for donor variability. P-values were generated by performing a two-way ANOVA with Fisher's Least Significant Difference (LSD) test. (H) Gating strategy used to analyze HIV_{DFII} infection profiles in the CD4+ CD73+/- T cell compartments. Data shown are from a single, mock-treated donor and are representative for all seven donors. (I) The average frequency of latently-infected cells was assessed in CD4+ CD73+/- T cells. Colored dots indicate individual donors. P-values were generated by performing a two-way ANOVA with Fisher's LSD test. P-value threshold for significance was at $p < 0.05$. Error bars show SEM.

CD73+ cells exhibit specific immunoregulation and tyrosine kinase signaling cascade patterns. The role of CD73 in the context of oncogenesis, tumor progression and survival is well described[36]. Hitherto however, relatively little is known about the relevance and function of CD73 in human CD4+ T cells. We thus characterized the transcriptome of blood-derived, primary CD73+ and CD73- CD4+ T cells by RNA sequencing. To this aim, CD73-/+ cells were isolated from primary CD4+ T cells by FACS, revealing highly variable CD73 surface expression on CD4+ T cells across donors, ranging from ~3% to ~23% (Figure S4A and B). Sorted cells were then subjected to RNA sequencing and analyzed for DGE, taking into account and adjusting for donor effects (Figure S4C and D). CD73- and CD73+ CD4+ T cells exhibited distinct transcriptional profiles and a clear clustering of the sorted populations (Figure 5A). Expectedly, CD73 showed the most significant DGE, and we found 145 additional genes being differentially expressed, with 111 upregulated and 34 downregulated genes in CD73+ cells (Figure 5B). *CR1, ADAM23, ABCB1 and AUTS2* were among the top genes upregulated in CD73+ cells (Figure 5B, yellow dots). *CLEC17A* exhibited the highest fold change (> 5-fold),

followed by *CD73, LINC02397* and *MACROD2* (> 4-fold) (Figure 5B, red dots). Multiple genes were markedly downregulated in CD73+ cells; however, only two of them reached the highest level of statistical significance: *FCER1A* and *NPR3*. A gene set enrichment analysis yielded a multitude of significantly changed pathways between CD73+ and CD73- cells including 'immune responses', 'complement activation' and 'receptor-mediated signaling cascades' (Figure 5C) indicating diverging immunoregulatory programs being active in CD73+ and CD73- cells. In addition, 'positive regulation of angiogenesis', 'regulation of apoptotic processes' and 'tyrosine kinase signaling cascades' were among the 40 most significantly changed pathways.

Next, all differentially expressed hits were uploaded into Cytoscape and the resulting protein-protein interaction network was then overlaid with $\log_2$ fold changes and adj. p-values of each gene, visualizing directionality and significance of interacting hits (Figure 5D). The analysis revealed 5 distinct interaction networks, with one network containing the majority of hits. This intrinsically cross-connected network pointed towards overlapping signaling cascades and biological processes shared by the entire CD73+ CD4+ T cell compartment. Within this network, a tight cluster (I) of cell surface receptors was apparent (*CD22, CD79A, CR1, CR2, KIT, FCER1A, CD34*), accompanied by several signaling factors (*LYN, BLNK, BLK, BTK, PIK3AP1, TCL1A)* and transcription factors (*IRF8, EBF1, PAX5*). Another cluster (II) comprised downregulation of cell surface proteins *CXCR3*, *CCR4* and *PTGDR2*. Importantly, the network also contained two significantly downregulated genes, transcription factor *GATA2*, and DNA topoisomerase *TOP2A*, which are known to support active HIV transcription and replication[43,44].

CD73+ CD4+ T cells harbor an inducible HIV reservoir. The intactness of integrated proviruses and the inducibility of viral gene expression are key determinants of the latent HIV reservoir. We therefore sought to investigate the capability of the HIV reservoir in CD73+ T cells to support reactivation of viral

transcription. To this end, we adapted a primary *in vitro* HIV infection model[45] and infected FACS-sorted CD73- and CD73+ CD4+ T cells with the reporter virus HIV_{Luc} (Figure 5E). After a resting period of 5 days, we stimulated cells with αCD3/αCD28 beads and observed a pronounced increase of viral transcription in both, CD73- and CD73+ CD4+ T cells as compared to unstimulated cells, reflected by a 10-fold and 14-fold increase in LTR-driven luciferase activity, respectively (Figure 5F). Interestingly, induction of viral transcriptional activity was significantly higher in stimulated CD73+ T cells as compared to CD73- T cells. These results demonstrate that the CD73+ CD4+ T cell compartment can harbor an inducible latent reservoir *in vitro*, indicating the potential of this compartment to contribute to a spreading infection in PLWH upon treatment cessation.

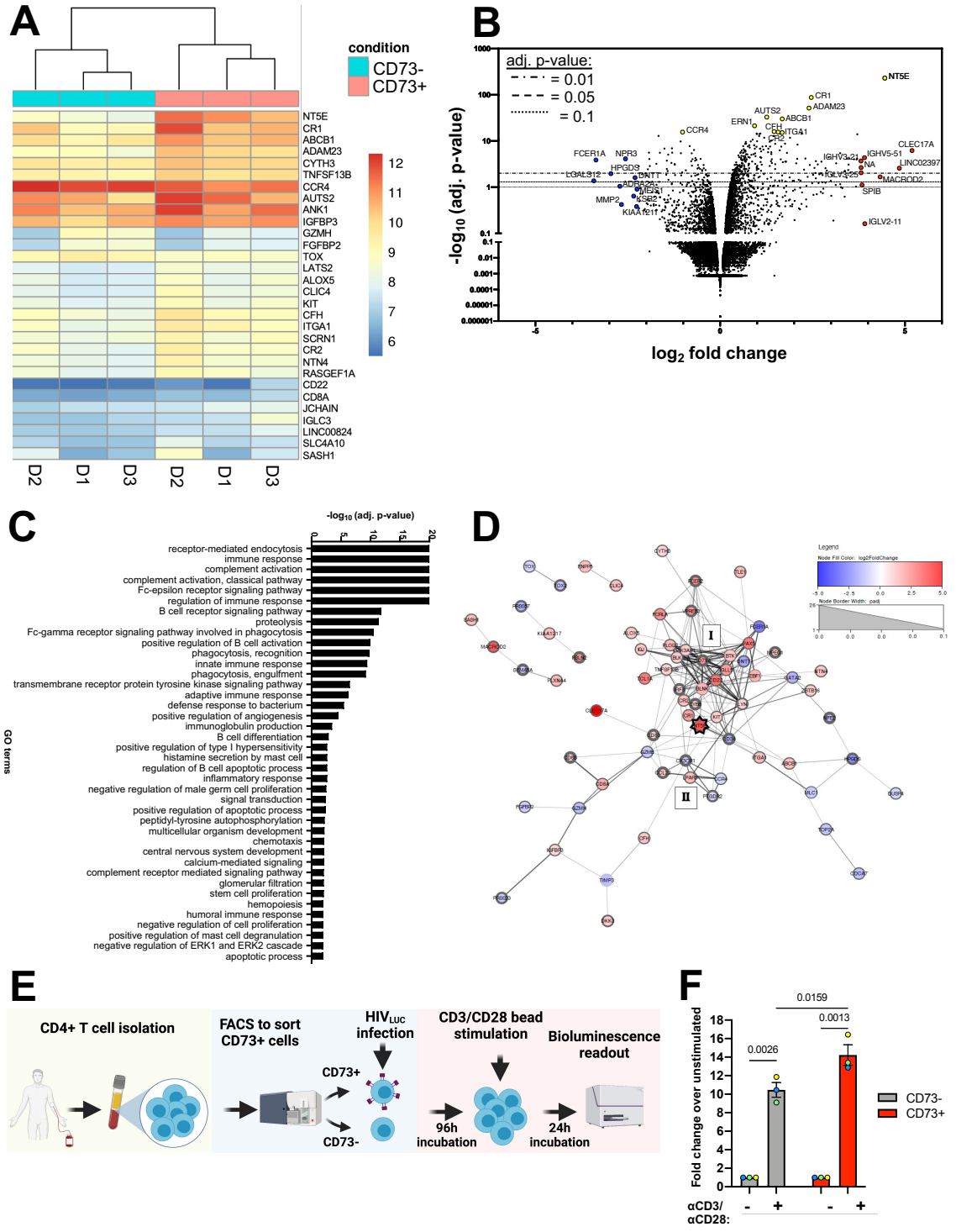

Figure 5: CD73+ cells feature specific immunoregulation and signaling cascade patterns and support reactivated viral transcription. (A) Clustering heatmap visualizing the expression profile of the top 30 differentially expressed genes sorted by their adjusted p-value. Data were adjusted for the donor effect. (B) Global transcriptional changes between CD73- and CD73+ cells are visualized in the volcano plot. Each data

point represents a single gene. The log_2 fold change of the normalized mean hit counts of each gene are plotted against $-log_{10}$ of its adj. p-value (using the Benjamini-Hochberg method). Horizontal lines indicate adj. p-value thresholds. The top 10 most significantly changed (yellow), most upregulated (red) and most downregulated (blue) genes are highlighted. (C) Differentially expressed genes were grouped by their gene ontology (GO) and the enrichment of GO terms was tested using Fisher exact test. The top 40 GO terms with an adj. p-value < 0.05 are displayed. (D) The protein-protein interaction network of genes differentially expressed between CD73- and CD73+ CD4+ T cells was generated in Cytoscape as described before. 33/145 hits were not recognized by the STRING database and thus excluded from the interaction network. Among the remaining 112 genes, 43 genes did not have an interaction partner and are not displayed. Log_2 fold changes of genes are indicated by node pseudo color and the adj. p-value by node border width. *CD73* (*NT5E*) is highlighted by a star shape. Protein clusters of interest are labeled. (E) The schematic represents the experimental workflow to test reactivation of integrated provirus in sorted CD73- and CD73+ CD4+ T cells. (F) Bars display the average fold change over unstimulated cells from three donors. Colored dots indicate individual donors. P-values above bars were generated by performing a two-way ANOVA with Fisher's LSD. A p-value at $p < 0.05$ was considered significant. Error bars show SEM.

Blocking the adenosine receptor A2AR promotes HIV latency reversal. Bearing in mind the enzymatic function of CD73, we hypothesized that extracellular adenosine produced by CD73 could be mechanistically involved in the establishment and/or maintenance of HIV latency. To test this, we investigated the adenosine signaling cascades downstream of CD73 in well-established cell line models[46,47] of latency, the so-called J-Lat cells[46,47], exploring how modulation of adenosine receptors by small molecule drugs affects HIV transcriptional activity.

First, CD73 surface expression was measured in three J-Lat clones, 5A8, 6.3 and 11.1, as well as in the parental JurkatE6 cell line (Figure 6A). Between 10-20% of JurkatE6, J-Lat 6.3 and 11.1 cells expressed CD73 on the surface. In strong contrast, about 80% of J-Lat 5A8 cells were CD73 positive. Due to this remarkably high frequency of CD73-expressing cells, subsequent experiments were performed with this clone. J-Lat 5A8 cells were pretreated with the antagonist SCH-58261 (SCH), which blocks adenosine signaling, followed by viral reactivation with PMA/I, a strong mitogen and latency reversing agent. SCH pretreatment did not compromise cell viability at any dose compared to cells treated with PMA/I only (Figure 6B). Notably, pretreatment with SCH significantly promoted latency reversal

and resulted in an evident dose response with a 2-fold increase in the frequency of GFP+ cells at the highest dose (Figure 6C).

A comprehensive model of CD73-dependent latency. Based on our data, obtained in *in vitro* infection models and cell lines, we devised a model that incorporates hypoxia, CD73 and adenosine signaling, linking it with HIV transcriptional regulation and persistence. Our model predicts that the hypoxia-CD73-adenosine (HCA) axis plays a vital role with CD73 as a central player in the maintenance of latent HIV infection (Figure 6D): As is known, HIV preferentially persists in lymphatic tissues[48], which exhibit low oxygen levels and thus high levels of active HIFs. We surmise that the resulting upregulation of CD73 expression leads to adenosine-rich, immunosuppressive microenvironments, which promote the establishment and maintenance of latent reservoirs. Accumulation of extracellular adenosine thereby creates optimal conditions for HIV persistence by suppressing HIV host dependency factors through autocrine signaling cascades, while impairing effective host immune responses through paracrine signaling mechanisms. Therefore, viral transcription is repressed, and immune escape of HIV-infected cells is facilitated, altogether promoting viral quiescence and survival of the latent reservoir.

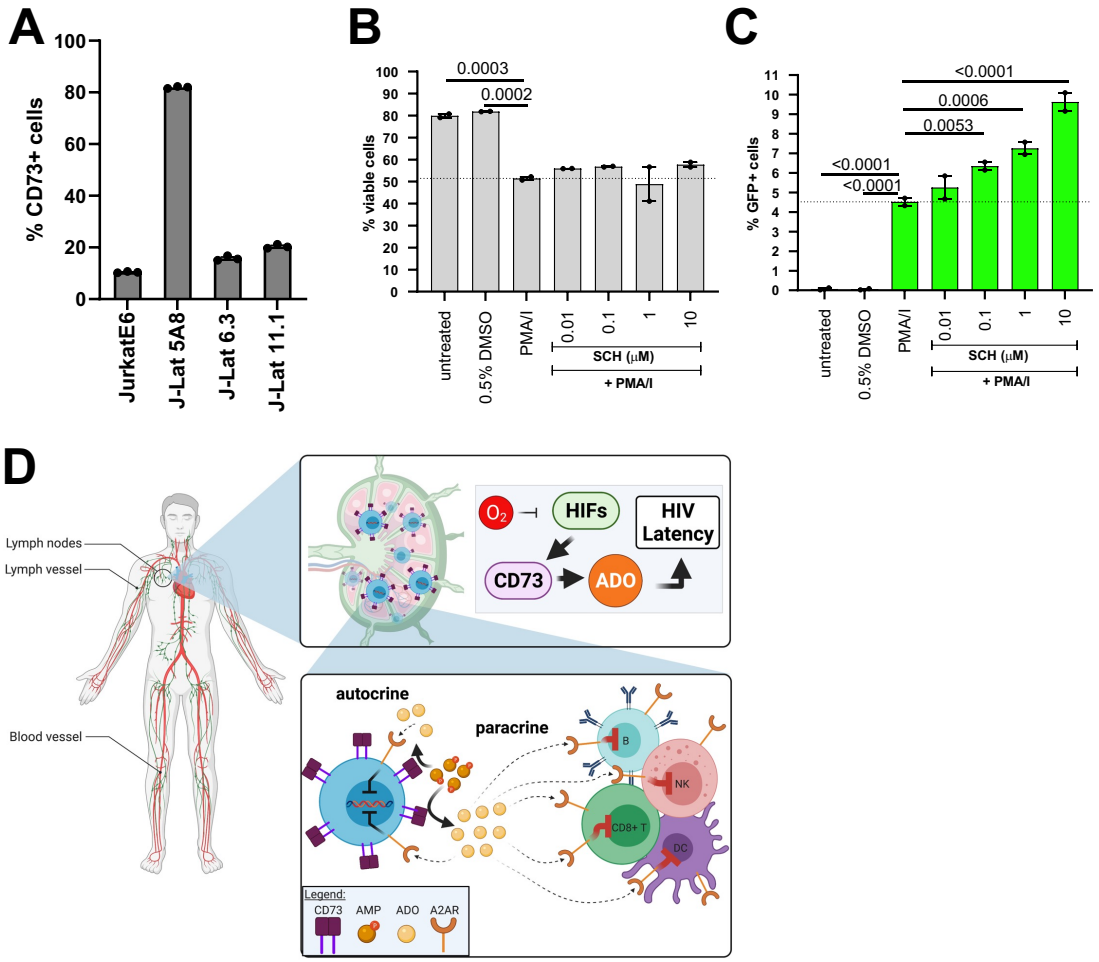

Figure 6: Blockade of adenosine receptor A2AR facilitates HIV latency reversal. (A) Average frequency of live, single CD73+ cells in the different T cell lines measured via flow cytometry. (B and C) J-Lat 5A8 cells were treated with A2AR antagonist SCH-58261 (SCH) at indicated, increasing doses for 1h, followed by treatment with PMA/I. PMA/I treatment alone served as positive control, 0.5% DMSO treatment as mock control. (B) Cell viability based on FSC-A and SSC-A and (C) GFP expression as a reporter of HIV transcriptional activity were assessed 7h post treatment using flow cytometry. Samples were measured in duplicates. P-values were generated by performing a one-way ANOVA with Fisher's LSD. A p-value at $p < 0.05$ was considered significant. Data represent the mean and error bars the SEM. (D) Under long-term ART, HIV persists *in vivo* preferentially in anatomical sanctuary sites like lymph nodes. Oxygen levels are known to be significantly lower in lymphoid tissues (0.5-4.5%) compared to the periphery (about 13%). Low oxygen supply or hypoxia lead to stabilization of hypoxia inducible factors (HIFs) which control the expression of CD73. Upregulation of CD73 leads to the accumulation of adenosine (ADO) in the extracellular space. These factors favor the establishment of viral reservoirs and promote HIV persistence, silencing the provirus through autocrine and inhibiting host immune responses by paracrine signaling mechanisms. T cells are shown in blue, CD73 in purple.

Detection of HIV and CD73 colocalization in patient-derived tissue. To evaluate the clinical relevance of our findings and to test the HCA model *in vivo*, we applied a comprehensive tissue imaging pipeline that enables simultaneous detection of integrated HIV-DNA, viral mRNA, and HIV protein, as well as lineage markers *in situ*, followed by quantitative image analyses[48]. We concomitantly detected CD73 expression and HIV molecules in lymph node tissues (peripheral and inguinal lymph nodes) obtained from HIV-infected individuals on suppressive ART, as well as in viremic untreated individuals, and uninfected controls (Figure 7A). CD3 staining was used as a lineage marker for T cells and DAPI was included as a counter staining of nuclear DNA. CD73 signals were found across all samples, while HIV detection expectedly differed greatly between ART-suppressed and viremic individuals and was absent in uninfected control samples (Figure 7A and B). The CD73 expression and distribution in uninfected lymph nodes was uniform (Figure 7A). In contrast, in the setting of HIV infection, CD73 was mostly concentrated in HIV-infected or surrounding cells (Figure 7A). Quantification of the viral reservoir in viremic individuals indicated that at least 40% of CD3+ cells harbored integrated DNA and most of these cells expressed viral RNA and HIV-p24 (Figure 7B, viremic). In contrast, in ART-suppressed individuals, 0.017% of CD3+ cells contained viral DNA, half of which expressed viral RNA and 10% of which expressed viral proteins (Figure 7B, ART-suppr.). No unspecific detection of viral DNA, RNA or protein were detected in uninfected tissues.

CD73 expression correlates with HIV persistence in lymph nodes from ART-suppressed individuals. Next, we assessed correlations between HIV infection at the cellular level and CD73 expression specifically in the CD3+/CD3- cell compartment (Figure 7C). In general, CD73 expression levels in CD3+ cells were significantly higher in ART-suppressed samples as compared to uninfected samples. In addition, HIV DNA+ CD3+ cells in ART-suppressed individuals possessed a significant, 1.6-fold higher CD73 expression compared to the overall

CD3+ population. This difference in CD73 expression levels was not observed in viremic individuals and suggested that CD73 expression might offer a survival advantage for HIV-infected cells in the setting of ART. We surmise that in the absence of treatment, when HIV is not subject to pharmacologic selection pressure, active viral replication dominates and potentially overwrites CD73 effects. It is likely that the long-term persistence of HIV during ART unearths the association between CD73 and viral latency. We further hypothesized that the effects of CD73-mediated viral persistence would not be limited to the CD73-expressing cell itself, and the immunosuppressive effects due to adenosine production would cover a 'neighborhood' within the lymph node. To explore this hypothesis, we performed analyses of the imaging data measuring distance-dependent CD73 positivity in the vicinity of CD3+ cells. Our data indicated that HIV DNA+ CD3+ cells in lymph nodes from ART-suppressed individuals reside in areas with generally high CD73 expression, reinforcing the notion that CD73 via adenosine production is contributing to HIV persistence (Figure 7D).

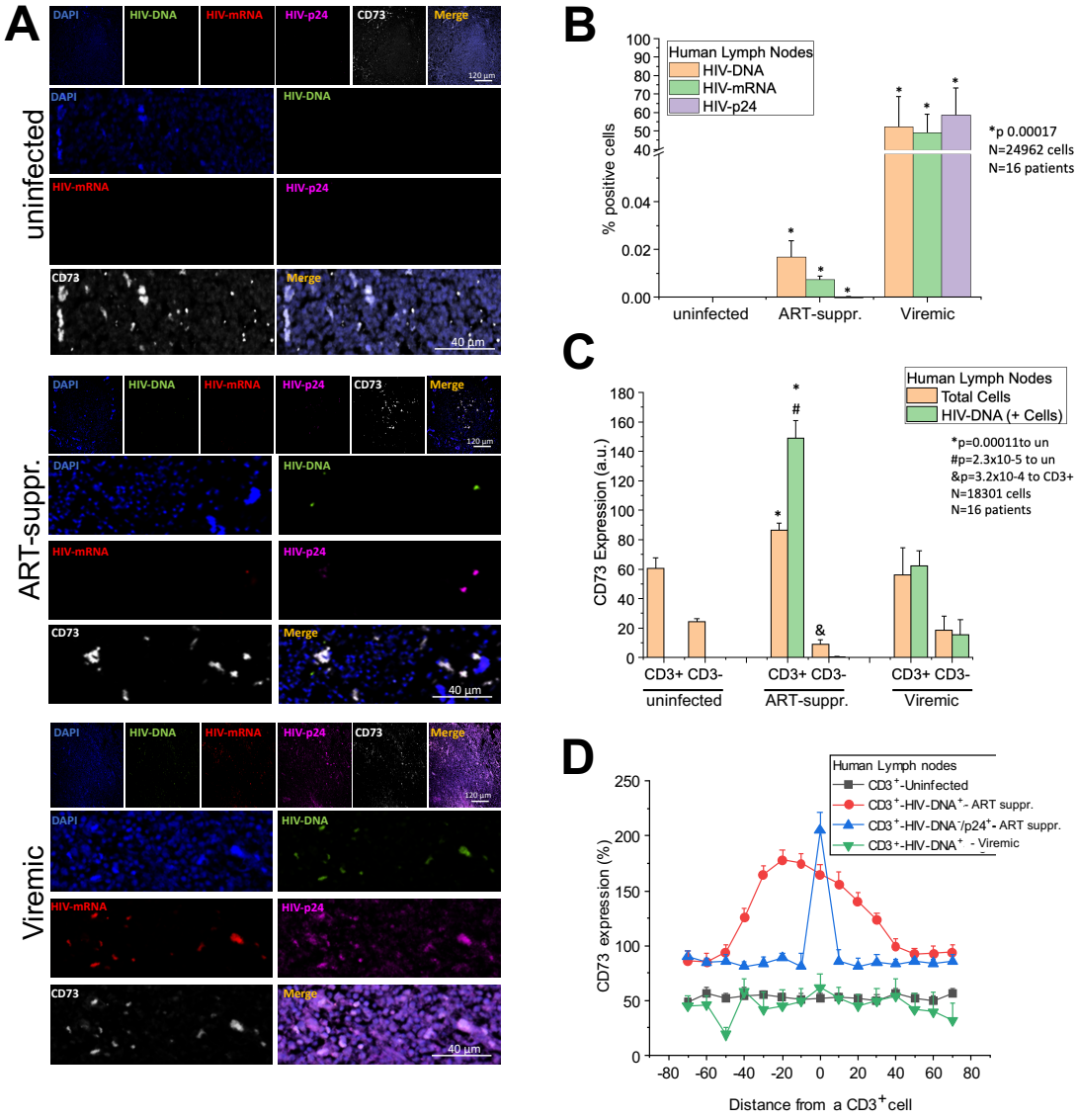

Figure 7: *In situ* imaging of lymph nodes from PLWH reveals associations between CD73 expression and HIV DNA specifically in ART-suppressed individuals. (A) Panels show representative confocal microscopy images for CD73 and HIV molecule staining of lymph node tissue obtained from uninfected, ART-suppressed (suppr.), and viremic individuals. (B) Automated image analysis of tissue sections stained for HIV DNA, mRNA and p24 protein in uninfected (n = 5), ART-suppressed (n = 6), and viremic individuals (n = 5). Bar graphs show the average percentage of cells that exhibit a positive signal for the respective target. (C) Quantitative CD73 expression analysis in tissue samples from uninfected (n = 5), ART-suppressed (n = 6) and viremic individuals (n = 5). Identification of the T cell compartment (CD3+ cells) and detection of HIV reservoir cells (HIV-DNA+) was followed by quantification of CD73 signals in the indicated 4 cellular subsets (CD3+ HIV-DNA-, CD3+ HIV-DNA+, CD3- HIV-DNA-, CD3 HIV-DNA+). ANOVA was used to compare the different groups. Relevant statistics are shown in the bar graphs. (D) The distance in µM of CD73 expression to CD3+ cells were determined for all 4 indicated cellular subsets.

DISCUSSION

The latent HIV reservoir is considered the main obstacle to achieving full remission from HIV infections. It is generally believed that integrated provirus persists in specific cellular compartments and tissue sanctuaries, which enable both, long-term survival and spontaneous reactivation of viral replication even after decades of successful ART. The exact identity of the HIV reservoir however remains elusive. Goal of this study was to thoroughly characterize primary HIV latently-infected cells using two comprehensive and complementary systems approaches. Our work focused on CD4+ T cells, the major target of HIV infection and an important source of viral rebound upon ART interruption.

The core finding of this work was the identification of an elevated cell-surface expression of CD73 as signature characteristic of HIV latently-infected CD4+ T cells – an observation that, to the best of our knowledge, has not been described before. Using different *in vitro* models of HIV latency, we found indications that CD73 is not just a passive marker of reservoir cells, but that the regulation of CD73 expression as well as its enzymatic function may be linked to HIV persistence.

Noteworthily, our NanoString analysis also indicated significant changes in the expression of CD39 and IL8, which are mechanistically connected. In particular the two ectonucleotidases CD39 and CD73, and their orchestrated functionality in purinergic signaling are well described in the literature[36–38]. In addition, IL8 expression has been shown to be stimulated by adenosine signaling, and is thus directly linked to the enzymatic function of CD73[35]. The distinctive expression of these three genes in latent cells suggest that CD73 and the adenosinergic pathway play a pivotal role in HIV latency and the establishment and/or maintenance of viral reservoirs.

Our initial *in vitro* infection model using HIV_{DFII} focused on a rather narrow time window of HIV latency, thus recapitulating the establishment and early persistence of viral reservoirs within a few days after infection. In clinical settings and most

infected individuals on the other hand, HIV persists even after decades of successful ART. In line with that, our *in situ* imaging of lymph node tissues demonstrated, for the first time, that a significant association between CD73 expression in T cells and HIV-DNA specifically in ART-suppressed individuals is being maintained over extended periods of time.

A key finding of our study is also that CD73 is significantly upregulated under hypoxic conditions in the CD4+ T cell compartment. This result is important for two reasons: 1) Oxygen tension levels are highly variable throughout the body, ranging from 19% in well oxygenated tissues[49], down to 0-7%[50] in the gastrointestinal tract, and 0.5-4.5% in lymphoid organs[51,52]. As a consequence, immune cells including CD4+ T cells encounter and operate at varying oxygen concentrations as they traffic through the body[52]. Lymphoid organs in particular represent crucial viral sanctuaries and as these are characterized by low oxygen levels, our data suggest a causal link between HIV persistence, CD73 and hypoxia. 2) Hitherto, the role of oxygen levels and hypoxia in HIV infection remains intangible and somewhat obscure. In 2009 Charles et al.[53] reported decreased HIV-1 RNA levels at 3% oxygen, while S. Deshmane and colleagues showed increased HIV transcription mediated by the interaction between HIV accessory protein Vpr and HIF-1α[54,55]. Moreover, HIV-1 replication was shown to be promoted by HIF-1α which in turn was stabilized by reactive oxygen species[56]. Very recently it was demonstrated that hypoxia can promote HIV latency with HIF-2α as a direct inhibitor of viral transcription[57]. Our data now provided new insights into the connection between HIV latency and hypoxia, with CD73 emerging as key mediator between hypoxia and viral transcription.

As outlined above, the clear association between CD73 expression and HIV latency suggested a mechanistic involvement of CD73 via its enzymatic function in the adenosine signaling cascade. Adenosine signaling leads to a suppression of cellular transcription factors that are critical for active viral transcription[58,59] and may create

an ideal immunological niche for infected cells to evade host immune clearance due to an adenosine-mediated immunosuppressive microenvironment. In fact, pharmacological blockade of A2AR in an HIV latency cell culture system clearly facilitated HIV latency reversal without impairing cell viability. Thus, our data demonstrate the potential of targeting the adenosinergic system as a therapeutic approach in the context of HIV infection and provides first evidence that the enzymatic activity of CD73 is directly involved in HIV persistence.

It is important to note that in recent years increasing circumstantial evidence has been gathered, independently suggesting a critical role for either hypoxia[53–57], CD73 expression[60–62] or adenosine signaling[63–67] in HIV infections. Our data now implies a direct, causal connection that links the hypoxic regulation and adenosine-producing enzymatic activity of CD73 to the establishment and persistence of viral reservoirs.

Finally, the CD73-adenosine axis has received a great deal of attention in the context of cancer biology[68–70] and the adenosinergic system has emerged as a promising new drug target in oncology[35,36,71–76]. Our data suggest that, like solid tumor cells, latent HIV reservoirs hijack the CD73-adenosine axis to subvert innate and adaptive immune responses, enhancing the survivorship of the infected cell as a persistence mechanism during ART. Therefore, CD73- and adenosine-focused anti-cancer therapeutics should be actively explored for the development of novel HIV cure approaches and host-directed therapies.

MATERIALS AND METHODS

Molecular Cloning. The 1st generation dual reporter virus construct R7GEmC[24] (kindly provided by Dr. Eric Verdin) was adapted by ligation-based molecular cloning. Briefly, R7GEmC was linearized by enzymatic digest using FseI and AscI (New England Biolabs, Cat. #R0588S and Cat. #R0558S) in order to excise the mCherry open reading frame. Then, mKO2 was PCR amplified from the template mKO2-N1 (Addgene, Cat. #4625) using primers containing matching restriction sites. Subsequently, the lentiviral vector was dephosphorylated using Quick CIP (New England Biolabs, Cat. #M0525S), purified and subjected to ligation with the digested and gel-purified PCR product utilizing T4 DNA ligase (New England Biolabs, Cat. # M0202S). Finally, circularized plasmid DNA was transformed by heat-shock in chemically competent Stbl-3 E. coli (ThermoFisher Scientific, Cat. #C737303) for subsequent antibiotics selection and Sanger sequencing (Elim Biopharm) of positive clones.

Plasmid amplification and preparation. Transformed Stbl-3 cells were grown in 2-5 ml of lysogeny broth with 0.1 mg/ml Ampicillin (LB Amp) for 4-8 hours prior to inoculation of large-volume flask with 100-300 ml LB Amp for overnight growth. 16 hours later, cells were pelleted by centrifugation for 15 min at >3000 g and subjected to plasmid preparation using Plasmid Plus Maxi Kits (QIAGEN, Cat. #12963) following the manufacturer's protocol. The DNA concentration of isolated plasmid DNA was spectrophotometrically determined using a NanoDrop 1000 (ThermoFisher, Scientific) and DNA aliquots were stored at 4°C.

Cell lines and cell culture. HEK293T were obtained from ATCC and were cultured in DMEM (ThermoFisher, Scientific, Cat. # 11965-118) supplemented with 10% FBS (Corning, Inc., Cat. #35-010-CV) and 10% Penicillin/1% Streptomycin (Fisher Scientific, Cat. #11548876) (DMEM complete = DMEM+/+) at 37°C, 5% CO_2 unless stated otherwise. J-Lat 5A8 cells were kindly provided by Warner C. Greene (Gladstone Institutes). All other J-Lat clones were a gift from Eric Verdin (Buck

Institute). Jurkat E6-1 cells were obtained from ATCC. All suspension cells were cultured in RPMI 1640 (ThermoFisher, Scientific, Cat. #11875-119) supplemented with 10% FBS and 10% Penicillin/1% Streptomycin (RPMI complete = RPMI+/+) at 37°C, 5% CO_2 unless stated otherwise.

Virus production. HIV-1 viruses were generated by transfection of proviral DNA into HEK293T cells via polyethylenimine (PEI, Polysciences, Cat. #23966) transfection protocol. Env-pseudotyped HIV_{DFII} stocks were produced by co-transfecting plasmids encoding HIV_{DFII} and a plasmid encoding HIV-1 dual-tropic envelope (pSVIII-92HT593.1, NIH HIV Reagent Program, Cat. #3077) at a ratio of 3:1 into HEK293T cells at 50-60% confluency grown in 175 cm^2 culture flasks. Each flask was transfected with a total amount of 30 µg DNA. The transfection mix was prepared in 2 ml Opti-MEM (ThermoFisher Scientific, Cat. #31985062) as follows: DNA plasmids were diluted in Opti-MEM first, then PEI was added at a ratio of 3:1 PEI:DNA (90 µg PEI). The transfection mix was vortexed for 15 sec and incubated for 15 min at RT. Culture medium was replaced with 20 ml fresh DMEM + 10% FBS <u>without P/S</u>, and 2 ml transfection mix was added to each flask. 16h post transfection, P/S-free medium was replaced with standard culture medium (DMEM+/+), and cells were incubated for another 24h at 37°C, 5% CO_2. For replication competent HIV NL4-3 Luciferase (a kind gift from Dr. Warner Greene), lentiviral vectors were introduced by Fugene HD transfection (Promega, Cat. #E2311) according to the manufacturer protocols. Cell supernatants were collected 48h post transfection, centrifuged at 4°C for 10 min at 4000 rpm (~ 3390 x g) and subsequently filtered using 0.22 µm membrane vacuum filter units (MilliporeSigma, Cat. #SCGP00525) to remove cell debris. Virus preparations were concentrated by ultracentrifugation at 20,000 rpm (~ 50,000 x g) for 2h at 4°C and resuspended in complete media for subsequent storage at -80°C. Virus concentration was estimated by p24 titration (HIV-1 alliance p24 ELISA kit, PerkinElmer, Cat. #NEK050001KT).

J-Lat cell latency reversal. J-Lat 5A8 cells (seeded at $1x10^6$ cells/ml) were incubated with CGS21680 (Sigma-Aldrich, Cat. #C141-5MG) or SCH-58261 (Sigma-Aldrich, Cat. #S4568-5MG) at 37°C for 1h at increasing doses in RPMI+/+, followed by stimulation with 20 nM PMA / 1 µM Ionomycin (PMA/I, Sigma-Aldrich, Cat. #10634-1MG and Cat. #10634-1MG). Untreated cells or cells treated with 0.5% DMSO (Sigma-Aldrich, Cat. #D2650-100ML) served as negative controls. 7h after PMA/I reactivation, cells were washed 2x with PBS (ThermoFisher, Scientific, Cat. #14190-250) and viral transcriptional activity, reflected by GFP expression was measured using LSR II flow cytometer (BD Biosciences).

Leucocyte isolation and primary cell culture. Peripheral blood mononuclear cells (PBMCs) from HIV-seronegative donors (Vitalant) were isolated by Ficoll-Hypaque density gradient centrifugation (Corning, Inc., Cat. #25-072-Cl) at 2000 rpm (~ 850 x g) at RT for 30 min, without brake. PBMCs were immediately processed to isolate CD4+ T cells by negative selection using the EasySep Human CD4+ T Cell Isolation Cocktail (StemCell Technologies, Cat. #17952) according to manufacturer's protocol. Purified CD4+ T cells were cultured in RPMI+/+.

CD4+ T cell *in vitro* activation and infection. CD4+ T cells from peripheral blood were stimulated with αCD3/αCD28 activating beads (ThermoFisher Scientific, Cat. #11132D) at a concentration of 1 bead/cell in the presence of 100 U/ml IL-2 (PeproTech, Inc., Cat. #200-02) in RPMI +/+ for 3 days (initial seeding concentration $1x10^6$ cells/ml). At the day of infection, cells were spinoculated in 96-well V-bottom plates (MilliporeSigma, Cat. #M9686-100EA) in 50 µl RPMI+/+ with 100 ng (HIV_{DFII}) of p24 per 1×10^6 cells with 5×10^6 cells total per well for 2 h at 2350 rpm (1173 × g) at 37°C. After spinoculation, all cells were returned to culture in the presence of 30 U/ml IL-2. Pre-stimulated CD4+ T cells stayed in αCD3/αCD28 activating beads during spininfection and subsequent cell culture. For hypoxia experiments, cells were treated with 500 µM DMOG (Sigma-Aldrich, Cat. #D3695) or mock-treated with 0.5% DMSO two days after αCD3/αCD28 bead stimulation and 24h before

HIV_{DFII} spininfection. Cells were kept in DMOG containing RPMI+/+, in presence of activation beads and IL-2 until sample collection 4 days post infection.

CD4+ T cell *in vitro* infection and latency reversal. Initially, CD4+ T cells were isolated from peripheral blood as described above and subjected to FACS of CD73+ and CD73- cells. To that aim, cells were stained with APC anti-human CD73 (BioLegend, Cat. #344006) diluted in PBS (1:20) in 100 µl final volume for 20 min at RT. Cells were then washed twice with PBS and resuspended in 500 µl – 1000 µl PBS to achieve high cell concentrations (20 - $40x10^6$ cells/ml) for FACS. Cells were sorted into 15 ml conical tubes containing 1.5 ml RPMI+/+. Cells were cultured for 24h, then infected and rested in the presence of ART to establish *in vitro* latency[45]. Briefly, 100 ng of purified NL4-3-Luciferase was added per $1x10^5$ sorted cells, which were then infected by spinoculation as described above. 24h post virus exposure, 5 µM saquinavir (protease inhibitor, Sigma-Aldrich, Cat. #S8451-50MG) was added to the cell cultures to suppress spreading infection. 5 days later, cells were stimulated with αCD3/αCD28 beads (or left untreated) in the presence of 30 µM raltegravir (integrase inhibitor, Sigma-Aldrich, Cat. #CDS023737-25MG) to prevent new infections. 24h after stimulation, luciferase activity was quantified using the bright glo luciferase assay system (Promega, Cat. #E2610).

Cell staining and processing. Freshly isolated CD4+ T cells were stained for viability, using the fixable Zombie viability dye (1:100; BioLegend, Cat. #423113) according to the manufacturer's protocol. Subsequently, antibodies APC anti-Human CD73 (1:50), APC-Cy7 anti-Human CD25 (1:100, BD Pharmingen Cat. #557753), and V450 anti-Human CD69 (1:100, BD Horizon Cat. #560740) for cell surface staining diluted in PBS were added and incubated for 20 min at RT. For flow cytometry, cells were washed and fixed in 1% paraformaldehyde (PFA) in PBS after the staining. FACS experiments were performed with live, unfixed cell samples. Flow cytometry analyses were performed on the LSR II flow cytometer (BD Biosciences)

or MA900 Multi-Application Cell Sorter (Sony Biotechnologies). All fluorescent-based sorts were conducted on the latter instrument.

Flow cytometry gating and data analysis. Data were analyzed and visualized using the FlowJo software (v.10.7.1). Crosstalk compensations was performed using single-stained samples for each of the fluorochromes and isotype controls were employed to assess antigen positivity and enable specific gating. FACS and flow cytometry gating was performed as follows: first, single live cells were selected from FSC/SSC scatter plots, sub-gated on Zombie low/negative cells. Then, antibody gates (CD73, CD69 or CD25) were defined based on suited isotype controls. Gating of HIV_{DFII} reporter expression was based on non-infected, mock-treated (*in vitro* activated) negative control samples to account for activation-dependent increase of cellular background fluorescence.

Expression Profiling via NanoString. Quantitative RNA and protein expression data were generated using the nCounter Vantage 3D RNA:Protein Immune Cell Profiling Assay (NanoString Technologies, Inc., Cat. #121100019) and the nCounter SPRINT profiler (NanoString Technologies), comprising 770 RNA and 30 protein targets as well as positive and negative controls. 100,000 viable, sorted cells were used per sample, which were processed according to the manufacturer's instructions. RNA and protein expression values were normalized and analyzed using the nSolver Analysis Software 4.0 and the add-on Advanced Analysis Software 2.0.115 (NanoString Technologies). Samples that did not pass the default control performance and quality parameters were excluded from subsequent analysis. Normalization genes for each sample were automatically selected by the software based on the geNorm algorithm. Biological replicates were grouped according to sample type and the differential expression of each analyte-type (RNA or protein target) was determined in cross-comparisons among all sample types by considering inter-donor differences as confounding variable unless otherwise stated. Intersections of significant targets of individual differential expression

analyses were visualized in a Venn diagram using an open source platform from Bioinformatics & Evolutionary Genomics[77].

Based on the differential expression of each gene, gene sets pre-defined by nanoString, representing different pathways included in this assay, were analyzed by calculating global significance scores for each gene set within each sample as follows: undirected global significance statistic = $\left(\frac{1}{p}\sum_{i=1}^{p} t_i^2\right)^{\frac{1}{2}}$, where ti is the t-statistic from the ith pathway gene. The directed global significance statistic is similar to the undirected global significance statistic, but rather than measuring the tendency of a pathway to have differentially expressed genes, it measures the tendency to have over- or under-expressed genes. It is calculated similarly to the undirected global significance score, but it takes the sign of the t-statistics into account: Directed global significance statistic = $sign(U)|U|^{1/2}$ where U = $\left(\frac{1}{p}\sum_{i=1}^{p} sign(t_i) * t_i^2\right)$ and where sign(U) equals -1 if U is negative and 1 if U is positive (MAN-10030-02[78]).

CyTOF samples preparation and analysis. For live/dead discrimination, 0.1-1 million cells per sample were treated with cisplatin (Sigma-Aldrich) and fixed with paraformaldehyde (PFA) as previously described[9,26,27]. Briefly, Cells were washed once with contaminant-free PBS (Rockland) with 2 mM EDTA (Corning), centrifuged and resuspend with 25 μM cisplatin in 4 ml PBS/EDTA and incubated for 60 seconds at room temperature, and then quenched with CyFACS (metal contaminant-free PBS supplemented with 0.1% bovine serum albumin and 0.1% sodium azide). Cells were then centrifuged, fixed with 2% PFA in metal contaminant-free PBS and washed 3x with CyFACS. These fixed cells were stored at -80°C until CyTOF staining.

Prior to CyTOF staining, multiple samples were barcoded using the Cell-ID 20-Plex Pd Barcoding Kit according to manufacturer's instructions (Fluidigm). Briefly, each sample was washed twice with Barcode Perm buffer (Fluidigm), and incubated for

30 min with the appropriate barcode at a 1:90 ratio. Cells were then washed with 0.8 ml Maxpar Cell Staining buffer (Fluidigm) in Nunc™ 96 Deep-Well polystyrene plates (Thermo Fisher), followed by CyFACS. Barcoded samples were combined and blocked with sera from mouse (Thermo Fisher), rat (Thermo Fisher), and human (AB serum, Sigma-Aldrich) for 15 minutes at 4°C. Cells were washed twice with CyFACS buffer and stained with the cocktail of CyTOF surface staining antibodies (Table S1) for 45 min on ice. Subsequently, cells were washed 3X with CyFACS buffer and fixed overnight at 4°C with 2% PFA (Electron Microscopy Sciences) in metal contaminant-free PBS. For intracellular staining, cells were permeabilized by incubation with fix/perm buffer (eBioscience) for 30 min at 4°C and washed twice with Permeabilization Buffer (eBioscience). Cells were blocked again with sera from mouse and rat for 15 min on ice, washed twice with Permeabilization Buffer (eBioscience), and stained with the cocktail of CyTOF intracellular staining antibodies (Table S1) for 45 min on ice. Cells were then washed once with CyFACS and incubated for 20 min at room temperature with 250 nM Cell-IDTM DNA Intercalator-Ir (Fluidigm) in 2% PFA diluted in PBS. Cells were washed twice with CyFACS, once with Maxpar Cell Staining Buffer (Fluidigm), once with Maxpar PBS (Fluidigm), and once with Maxpar Cell Acquisition Solution (CAS, Fluidigm). Immediately prior to acquisition, cells were resuspended in EQTM calibration beads (Fluidigm) diluted in CAS. Cells were acquired at a rate of 250-350 events/sec on a CyTOF2 instrument (Fluidigm) at the UCSF Parnassus single cell analysis facility.

Data were normalized to EQTM calibration beads and de-barcoded with CyTOF software (Fluidigm). Normalized data were imported into FlowJo (BD) for gating (cell, intact, live, single events) and heatmap was generated in Cytobank.

RNA Sequencing. Freshly isolated CD4+ T cells from healthy blood donors were sorted based on their CD73 expression as described above. $3x10^6$ cells were collected per sample and stored as dry cell pellets at -80 °C. RNA preparation, library preparation and mRNA sequencing were conducted at Genewiz (USA).

Paired-end sequencing was performed using the Illumina NovaSeq 6000 instrument to obtain a minimum of 20 million read pairs per sample with a read length of 2x150 bp. Sequence reads were trimmed to remove possible adapter sequences and nucleotides with poor quality using Trimmomatic v.0.36. The trimmed reads were mapped to the Homo sapiens GRCh38 reference genome available on ENSEMBL using the STAR aligner v.2.5.2b. Unique gene hit counts were calculated by using featureCounts from the Subread package v.1.5.2. The hit counts were summarized and reported using the gene_id feature in the annotation file. Only unique reads that fell within exon regions were counted. After extraction of gene hit counts, the gene hit counts table was used for downstream differential expression analysis. Using DESeq2, a comparison of gene expression between samples was performed adjusting for the donor effect as confounding variable. The Wald test was used to generate p-values and $\log_2$ fold changes. Genes with an adjusted p-value < 0.05 (Benjamini-Hochberg method) and absolute $\log_2$ fold change > 1 were called as differentially expressed genes for each comparison. A gene ontology analysis was performed on the statistically significant set of genes by implementing the software GeneSCF v.1.1-p2. The goa_human GO list was used to cluster the set of genes based on their biological processes and determine their statistical significance. A list of genes clustered based on their gene ontologies was generated.

***In Situ* Detection of HIV and Cellular Markers.** The experimental procedure for the immunofluorescence staining and parallel detection of viral nucleic acids has been described and gradually optimized in a series of previous publications[48,79,80]. In its ultimate version, the protocol enables the detection of HIV-integrated DNA, viral mRNA, viral proteins, and several cellular markers in the same assay. Sample preparation, data acquisition and subsequent analyses were conducted in the laboratory of Dr. Eliseo Eugenin.

Tissue samples. Tissues from ART-suppressed individuals who have been on treatment for at least 6 months and had viral loads below clinical detection limits (<50 RNA copies/ml), as well as tissues from HIV-negative and ART-naïve viremic individuals with high plasma loads (>50 RNA copies/ml) were part of an ongoing research protocol approved by University of Texas Medical Branch (UTMB). Further clinical data and additional information are available and will be provided upon request by the lead contact Eliseo Eugenin (eleugeni@utmb.edu). All tissues were obtained with full, written consent from the study participants and freshly collected specimens were immediately fixed with 4% PFA, then mounted into paraffin blocks and subjected to tissue sectioning and ultimately to analysis by immunostaining.

Staining procedures. Paraffin-embedded slides containing the tissue samples were consecutively immersed in the following solutions: xylene for 5 min (2 times), 100% EtOH for 3 min, 100% EtOH for 3 min, 95% EtOH for 3 min, 90% EtOH for 3 min, 70% EtOH for 3 min, 60% EtOH for 3 min, 50% EtOH for 3 min, miliQ H_2O for 3 min. Then, tissue was encircled with ImmEdge Pen to reduce the reagent volume needed to cover the specimens. Finally, slides were immersed in miliQ H_2O for 3 min. For Protein K treatment, tissues were incubated with proteinase K diluted 1:10 in 1X TBS (Fisher Scientific, Cat. #BP24711; and PNA ISH kit, Agilent Dako, Cat. #K5201) for 10 min at RT in a humidity chamber. Next, slides were immersed in miliQ H2O for 3 min, then immersed in 95% EtOH for 20 sec and finally, the slides were let air-dry for 5 min. For HIV DNA probe hybridization tissues were incubated with 10 μM PNA DNA probe for Nef-PNA Alexa Fluor 488 and Alu-PNA Cy5 (PNA Bio). Next, slides were placed in a pre-warmed humidity chamber and incubated at 42°C for 30 min, then the temperature was raised to 55°C for an additional 1 h incubation. Subsequently, tissues were incubated using Preheat Stringent Wash working solution (PNA ISH kit) diluted 1:60 in 1X TBS for 25 min in an orbital shaker at 55°C. Slides were equilibrated to RT by brief immersion in TBS for 20 sec. HIV mRNA detection followed the manufacturer's protocol for RNAscope 2.5 HD

Detection Reagent-RED (Advanced Cell Diagnostics, Inc., Cat. #322360). Probe for HIV Gag-pol was added to the tissue samples and incubated for 30 min at 42°C and then 50 min at 55°C. Next, samples were incubated in Preheat Stringent Wash working solution diluted 1:60 in 1X TBS (PNA ISH kit) for 15 min in an orbital shaker at 55°C. Finally, slides were immersed in 1X TBS for 20 sec. For HIV or cellular protein detection antigen retrieval was performed by incubating slide sections in commercial antigen retrieval solution (Agilent Dako, Cat. #S1700) for 30 min in a water-bath at 80°C. Next, slides were removed from the bath and allowed to cool down in 1X TBS. Samples were permeabilized with 0.1% Triton X-100 (Sigma-Aldrich, Cat. #X100) for 2 min and then washed in 1X TBS for 5 min three times. Unspecific antibody binding sites were blocked by incubating samples with freshly prepared blocking solution. Afterwards, sections were incubated overnight at 4°C using a humidity chamber (10 ml of blocking solution: 1 mL 0.5 M EDTA, 100 ul Fish Gelatin from cold water 45%, 0.1 g Albumin from Bovine serum Fraction V, 100 ul horse serum, 5% human serum, 9 mL miliQ H_2O). A primary antibody was added to the samples diluted in blocking solution and incubated at 4°C overnight. Then, slides were washed in 1X TBS 5 min for three times to eliminate unbound antibodies. Secondary antibodies were added at the appropriate dilutions and incubated for 2h at RT. Slides were washed three times in 1X TBS for 5 min to eliminate unbound antibodies. Next, slides were mounted using Prolong Diamond Antifade Mount medium containing DAPI (ThermoFisher Scientific, Cat. #P36931). Slides were kept in the dark at 4°C.

Image acquisition and analysis. Cells were examined by confocal microscopy using an A1 Nikon confocal microscope with spectral detection and unmixing systems. Image analysis was performed using the Nikon NIS Elements Advanced Research imaging software (Nikon Instruments Europe B.V.). The automated image segmentation and analysis is based on the following premises: For detection of HIV-integrated DNA, first, automatic or manual detection of cells that are positive

for HIV-DNA and second, the HIV-DNA probe has to colocalize with DAPI and Alu repeats staining with a Pearson's correlation coefficient of at least 0.8 as described previously[81]. For HIV-integrated DNA, these two conditions are essential, or the signal is considered negative or unspecific. For detection of HIV-mRNA, first, low colocalization with DAPI or Alu-repeats (0.2 Pearson's correlation coefficient or below) and second, presence in cells with HIV-DNA signal. The sensitivity, accuracy and specificity of the system was previously validated in the laboratory of our collaborator in two well characterized T cell lines A3.01 (uninfected) and ACH-2 (HIV-infected) and two monocytic cell lines, HL-60 (uninfected) and OM-10 (HIV-infected).

Quantification and Statistical Analysis. Statistical details are given in the figure legends. All statistical analyses were performed using GraphPad Prism software versions 9. P-values $\leq$ 0.05 were considered statistically significant. A Student's two-tailed t-test was used for two-way column analyses. ANOVA tests were used for multiple comparisons. P-values are denoted in figure panels. Data are presented as means with error bars indicating standard error of the mean (SEM) unless otherwise stated.

DATA AVAILABILITY

The datasets generated and/or analyzed during the current study are available from the corresponding author on reasonable request.

ACKNOWLEDGEMENTS

The authors would like to acknowledge Guorui Xie, PhD and Ashley George, PhD for helpful input regarding the CyTOF analysis. The authors thank Leonard Chavez, PhD and Shivani Desai for providing reagents, as well as Konstantinos Georgiou, PhD and Zain Y. Dossani, PhD for guidance and support in data analysis.

We would like to thank The National NeuroAIDS Tissue Consortium (NNTC) for providing all human samples and associated information. The NNTC is made possible through funding from the NIMH and NINDS by the following grants: Manhattan HIV Brain Bank (MHBB): U24MH100931; Texas NeuroAIDS Research Center (TNRC): U24MH100930; National Neurological AIDS Bank (NNAB): U24MH100929; California NeuroAIDS Tissue Network (CNTN): U24MH100928; and Data Coordinating Center (DCC); R01AI147777; R01AI127219; UM1AI64567; UM1AI64559. The staining and analysis were funded by the National Institute of Mental Health grant, MH096625 and MH128032 and the National Institute of Neurological Disorders and Stroke, NS105584 (to E. A. E.).

COMPETING INTERESTS

The authors declare no competing financial or non-financial interests.

REFERENCES

1. Ho, Y.-C. *et al.* Replication-Competent Noninduced Proviruses in the Latent Reservoir Increase Barrier to HIV-1 Cure. *Cell* **155**, 540–551 (2013).

2. Davey, R. T. *et al.* HIV-1 and T cell dynamics after interruption of highly active antiretroviral therapy (HAART) in patients with a history of sustained viral suppression. *Proc Natl Acad Sci U S A* **96**, 15109–15114 (1999).

3. Finzi, D. *et al.* Latent infection of CD4+ T cells provides a mechanism for lifelong persistence of HIV-1, even in patients on effective combination therapy. *Nature Medicine* **5**, 512–517 (1999).

4. Siliciano, J. D. & Siliciano, R. F. *Latency and viral persistence in HIV-1 infection*. *The Journal of Clinical Investigation* vol. 106 (2000).

5. Chun, T.-W. W. *et al.* Quantification of latent tissue reservoirs and total body viral load in HIV-1 infection. *Nature* **387**, 183–188 (1997).

6. Finzi, D. *et al.* Identification of a reservoir for HIV-1 in patients on highly active antiretroviral therapy. *Science (1979)* **278**, 1295–1300 (1997).

7. Wong, J. K. *et al.* Recovery of replication-competent HIV despite prolonged suppression of plasma viremia. *Science (1979)* **278**, 1291–1295 (1997).

8. WM, E.-S. *et al.* CD4+ Count–Guided Interruption of Antiretroviral Treatment. *New England Journal of Medicine* **355**, 2283–2296 (2006).

9. Neidleman, J. *et al.* Phenotypic analysis of the unstimulated in vivo hiv cd4 t cell reservoir. *Elife* **9**, 1–34 (2020).

10. Kulpa, D. A. & Chomont, N. HIV persistence in the setting of antiretroviral therapy: when, where and how does HIV hide? *Journal of Virus Eradication* **1**, 59–66 (2015).

11. Darcis, G., Berkhout, B. & Pasternak, A. O. The quest for cellular markers of HIV reservoirs: Any color you like. *Frontiers in Immunology* vol. 10 2251 (2019).

12. Fromentin, R. *et al.* CD4+ T Cells Expressing PD-1, TIGIT and LAG-3 Contribute to HIV Persistence during ART. *PLoS Pathogens* **12**, (2016).

13. McGary, C. S. *et al.* CTLA-4+PD-1− Memory CD4+ T Cells Critically Contribute to Viral Persistence in Antiretroviral Therapy-Suppressed, SIV-Infected Rhesus Macaques. *Immunity* **47**, 776-788.e5 (2017).

14. Iglesias-Ussel, M., Vandergeeten, C., Marchionni, L., Chomont, N. & Romerio, F. High levels of CD2 expression identify HIV-1 latently infected resting memory CD4+ T cells in virally suppressed subjects. *J Virol* **87**, 9148–58 (2013).

15. Serra-Peinado, C. *et al.* Expression of CD20 after viral reactivation renders HIV-reservoir cells susceptible to Rituximab. *Nature Communications* **10**, 1–15 (2019).

16. Hogan, L. E. *et al.* Increased HIV-1 transcriptional activity and infectious burden in peripheral blood and gut-associated CD4+ T cells expressing CD30. *PLOS Pathogens* **14**, e1006856 (2018).

17. Descours, B. *et al.* CD32a is a marker of a CD4 T-cell HIV reservoir harbouring replication-competent proviruses. *Nature* **543**, 564–567 (2017).

18. Pérez, L. *et al.* Conflicting evidence for HIV enrichment in CD32+ CD4 T cells. *Nature* **561**, E9–E16 (2018).

19. Osuna, C. E. *et al.* Evidence that CD32a does not mark the HIV-1 latent reservoir. *Nature* **561**, E20–E28 (2018).

20. Martin, G. E. *et al.* CD32-expressing CD4 T cells are phenotypically diverse and can contain proviral HIV DNA. *Frontiers in Immunology* **9**, 1 (2018).

21. Thornhill, J. P. *et al.* CD32 expressing doublets in HIV-infected gut-associated lymphoid tissue are associated with a T follicular helper cell phenotype. *Mucosal Immunology* **12**, 1212–1219 (2019).

22. Noto, A. *et al.* CD32 + and PD-1 + Lymph Node CD4 T Cells Support Persistent HIV-1 Transcription in Treated Aviremic Individuals . *Journal of Virology* **92**, 901–919 (2018).

23. Vasquez, J. J. *et al.* CD32-RNA Co-localizes with HIV-RNA in CD3+ Cells Found within Gut Tissues from Viremic and ART-Suppressed Individuals. *Pathogens and Immunity* **4**, 147 (2019).

24. Calvanese, V., Chavez, L., Laurent, T., Ding, S. & Verdin, E. Dual-color HIV reporters trace a population of latently infected cells and enable their purification. *Virology* **446**, 283–292 (2013).

25. Chavez, L., Calvanese, V. & Verdin, E. HIV Latency Is Established Directly and Early in Both Resting and Activated Primary CD4 T Cells. *PLOS Pathogens* **11**, e1004955 (2015).

26. Ma, T. *et al.* HIV efficiently infects T cells from the endometrium and remodels them to promote systemic viral spread. *Elife* **9**, 1–24 (2020).

27. Xie, G. *et al.* Characterization of HIV-induced remodeling reveals differences in infection susceptibility of memory CD4 + T cell subsets in vivo. *Cell Rep* **35**, (2021).

28. Kerkau, T., Gernert, S., Kneitz, C. & Schimpl, A. Mechanism of MHC Class I Downregulation in HIV Infected Cells. *Immunobiology* **184**, 402–409 (1992).

29. Cohen, G. B. *et al.* The selective downregulation of class I major histocompatibility complex proteins by HIV-1 protects HIV-infected cells from NK cells. *Immunity* **10**, 661–671 (1999).

30. Jacobs, M. D. & Harrison, S. C. Structure of an IκBα/NF-κB complex. *Cell* **95**, 749–758 (1998).

31. Ruelas, D. S. & Greene, W. C. An Integrated Overview of HIV-1 Latency. *Cell* **155**, 519–529 (2013).

32. Greene, W. C. & Peterlin, B. M. Charting HIV's remarkable voyage through the cell: Basic science as a passport to future therapy. *Nature Medicine* **8**, 673–680 (2002).

33. Doitsh, G. *et al.* Cell death by pyroptosis drives CD4 T-cell depletion in HIV-1 infection. *Nature* **505**, 509–514 (2014).

34. Allard, B., Allard, D., Buisseret, L. & Stagg, J. The adenosine pathway in immuno-oncology. *Nature Reviews Clinical Oncology* **17**, 611–629 (2020).

35. Kazemi, M. H. *et al.* Adenosine and adenosine receptors in the immunopathogenesis and treatment of cancer. *Journal of Cellular Physiology* **233**, 2032–2057 (2018).

36. Di Virgilio, F. & Adinolfi, E. Extracellular purines, purinergic receptors and tumor growth. *Oncogene* vol. 36 293–303 (2017).

37. Yegutkin, G. G., Henttinen, T., Samburski, S. S., Spychala, J. & Jalkanen, S. *The evidence for two opposite, ATP-generating and ATP-consuming, extracellular pathways on endothelial and lymphoid cells*. *Biochem. J* vol. 367 (2002).

38. Antonioli, L., Pacher, P., Vizi, E. S. & Haskó, G. CD39 and CD73 in immunity and inflammation. *Trends in Molecular Medicine* **19**, 355–367 (2013).

39. Hansen, K. R., Resta, R., Webb, C. F. & Thompson, L. F. Isolation and characterization of the promoter of the human 5′-nucleotidase (CD73)-encoding gene. *Gene* **167**, 307–312 (1995).

40. Fausther, M., Sheung, N., Saiman, Y., Bansal, M. B. & Dranoff, J. A. Activated hepatic stellate cells upregulate transcription of ecto-5=-nucleotidase/ CD73 via specific SP1 and SMAD promoter elements. *Am J Physiol Gastrointest Liver Physiol* **303**, 904–914 (2012).

41. Synnestvedt, K. *et al.* Ecto-5′-nucleotidase (CD73) regulation by hypoxia-inducible factor-1 mediates permeability changes in intestinal epithelia. *Journal of Clinical Investigation* **110**, 993–1002 (2002).

42. Kordaß, T., Osen, W. & Eichmüller, S. B. Controlling the immune suppressor: Transcription factors and MicroRNAs regulating CD73/NT5E. *Frontiers in Immunology* vol. 9 813 (2018).

43. Towatari, M., Kanei, Y., Saito, H. & Hamaguchi, M. Hematopoietic transcription factor GATA-2 activates transcription from HIV-1 long terminal repeat. *AIDS* **12**, 253–259 (1998).

44. Balakrishna, S. L., Satyanarayana, N. & Kondapi, A. K. Involvement of human topoisomerase II isoforms in HIV-1 reverse transcription. *Archives of Biochemistry and Biophysics* **532**, 91–102 (2013).

45. Lassen, K. G., Hebbeler, A. M., Bhattacharyya, D., Lobritz, M. A. & Greene, W. C. A Flexible Model of HIV-1 Latency Permitting Evaluation of Many Primary CD4 T-Cell Reservoirs. *PLoS ONE* **7**, e30176 (2012).

46. Jordan, A. HIV reproducibly establishes a latent infection after acute infection of T cells in vitro. *The EMBO Journal* **22**, 1868–1877 (2003).

47. Chan, J. K., Bhattacharyya, D., Lassen, K. G., Ruelas, D. & Greene, W. C. Calcium/Calcineurin Synergizes with Prostratin to Promote NF-κB Dependent Activation of Latent HIV. *PLoS ONE* **8**, e77749 (2013).

48. Prevedel, L. *et al.* Identification, Localization, and Quantification of HIV Reservoirs Using Microscopy. *Current Protocols in Cell Biology* **82**, 64 (2019).

49. Carreau, A., Hafny-Rahbi, B. El, Matejuk, A., Grillon, C. & Kieda, C. Why is the partial oxygen pressure of human tissues a crucial parameter? Small molecules and hypoxia. *Journal of Cellular and Molecular Medicine* **15**, 1239–1253 (2011).

50. Zenewicz, L. A. Oxygen Levels and Immunological Studies. *Frontiers in Immunology* **8**, 8–11 (2017).

51. Caldwell, C. C. *et al.* Differential Effects of Physiologically Relevant Hypoxic Conditions on T Lymphocyte Development and Effector Functions. *The Journal of Immunology* **167**, 6140–6149 (2001).

52. Ohta, A. *et al.* In vivo T cell activation in lymphoid tissues is inhibited in the oxygen-poor microenvironment. *Frontiers in Immunology* **2**, (2011).

53. Charles, S. *et al.* Regulation of HIV-1 transcription at 3% versus 21% oxygen concentration. *Journal of Cellular Physiology* **221**, 469–479 (2009).

54. Deshmane, S. L., Amini, S., Sen, S., Khalili, K. & Sawaya, B. E. Regulation of the HIV-1 promoter by HIF-1 and Vpr proteins. *Virology Journal* **8**, 1–7 (2011).

55. Deshmane, S. L. *et al.* Activation of the Oxidative Stress Pathway by HIV-1 Vpr Leads to Induction of Hypoxia-inducible Factor 1α Expression. *Journal of Biological Chemistry* **284**, 11364–11373 (2009).

56. Duette, G. *et al.* Induction of HIF-1α by HIV-1 Infection in CD4 + T Cells Promotes Viral Replication and Drives Extracellular Vesicle-Mediated Inflammation. *mBio* **9**, 1–21 (2018).

57. Zhuang, X. *et al.* Hypoxic microenvironment shapes HIV-1 replication and latency. *Communications Biology* **3**, (2020).

58. Romio, M. *et al.* Extracellular purine metabolism and signaling of CD73-derived adenosine in murine Treg and Teff cells. *American Journal of Physiology-Cell Physiology* **301**, C530–C539 (2011).

59. Sheridan, C. M., Heist, E. K., Beals, C. R., Crabtree, G. R. & Gardner, P. Protein kinase A negatively modulates the nuclear accumulation of NF-ATc1 by priming for subsequent phosphorylation by glycogen synthase kinase-3. *Journal of Biological Chemistry* **277**, 48664–48676 (2002).

60. Tóth, I. *et al.* Decreased frequency of CD73 + CD8 + T cells of HIV-infected patients correlates with immune activation and T cell exhaustion . *Journal of Leukocyte Biology* **94**, 551–561 (2013).

61. Schuler, P. J. *et al.* CD4+CD73+ T cells are associated with lower T-cell activation and C reactive protein levels and are depleted in HIV-1 infection regardless of viral suppression. *AIDS* **27**, 1545–1555 (2013).

62. Wang, X. *et al.* Decreased CD73+ Double-Negative T Cells and Elevated Level of Soluble CD73 Correlated With and Predicted Poor Immune Reconstitution in HIV-Infected Patients After Antiretroviral Therapy. *Frontiers in Immunology* **0**, 1445 (2022).

63. Li, J. *et al.* Reversal of the CD8+ T-Cell Exhaustion Induced by Chronic HIV-1 Infection Through Combined Blockade of the Adenosine and PD-1 Pathways. *Frontiers in Immunology* **12**, 1–11 (2021).

64. Nikolova, M. *et al.* CD39/Adenosine Pathway Is Involved in AIDS Progression. *PLoS Pathogens* **7**, e1002110 (2011).

65. He, T. *et al.* Critical Role for the Adenosine Pathway in Controlling Simian Immunodeficiency Virus-Related Immune Activation and Inflammation in Gut Mucosal Tissues. *Journal of Virology* **89**, 9616–9630 (2015).

66. Moreno-Fernandez, M. E., Rueda, C. M., Rusie, L. K. & Chougnet, C. A. Regulatory T cells control HIV replication in activated T cells through a cAMP-dependent mechanism. *Blood* **117**, 5372–5380 (2011).

67. Li, G. *et al.* Regulatory T Cells Contribute to HIV-1 Reservoir Persistence in CD4 + T Cells Through Cyclic Adenosine Monophosphate-Dependent Mechanisms in Humanized Mice in Vivo. *Journal of Infectious Diseases* **216**, 1579–1591 (2017).

68. Zhang, B. CD73 promotes tumor growth and metastasis. *OncoImmunology* vol. 1 67–70 (2012).

69. Chen, S. *et al.* CD73 expression on effector T cells sustained by TGF-β facilitates tumor resistance to anti-4-1BB/CD137 therapy. *Nature Communications* **10**, 1–15 (2019).

70. Vijayan, D. *et al.* Selective activation of anti-CD73 mechanisms in control of primary tumors and metastases. *OncoImmunology* **6**, e1312044–e1312044 (2017).

71. Allard, D., Chrobak, P., Allard, B., Messaoudi, N. & Stagg, J. Targeting the CD73-adenosine axis in immuno-oncology. *Immunology Letters* 1–9 (2018) doi:10.1016/j.imlet.2018.05.001.

72. Sek, K. *et al.* Targeting Adenosine Receptor Signaling in Cancer Immunotherapy. *International Journal of Molecular Sciences* **19**, 3837 (2018).

73. Leone, R. D. & Emens, L. A. Targeting adenosine for cancer immunotherapy. *Journal for ImmunoTherapy of Cancer* **6**, 57 (2018).

74. Chen, S. *et al.* CD73: an emerging checkpoint for cancer immunotherapy. *Immunotherapy* **11**, 983–997 (2019).

75. Antonioli, L., Yegutkin, G. G., Pacher, P., Blandizzi, C. & Haskó, G. Anti-CD73 in Cancer Immunotherapy: Awakening New Opportunities. *Trends in Cancer* **2**, 95–109 (2016).

76. Zhang, B. CD73: A Novel Target for Cancer Immunotherapy. *Cancer Research* **70**, 6407–6411 (2010).

77. Gent, U. of. Draw Venn Diagram. *Bioinformatics and Evolutionary Genetics* http://bioinformatics.psb.ugent.be/webtools/Venn/.

78. NanoString Technologies. nCounter Advanced Analysis 2.0 - User Manual. https://www.nanostring.com/application/files/2715/1789/8043/MAN-10030-03_nCounter_Advanced_Analysis_2.0_User_Manual.pdf (2018).

79. Ganor, Y. *et al.* HIV-1 reservoirs in urethral macrophages of patients under suppressive antiretroviral therapy. *Nature Microbiology* **4**, 633–644 (2019).

80. Real, F. *et al. Platelets from HIV-infected individuals on antiretroviral drug therapy with poor CD4 + T cell recovery can harbor replication-competent HIV despite viral suppression*. *Sci. Transl. Med* vol. 12 (2020).

81. Dunn, K. W., Kamocka, M. M. & McDonald, J. H. A practical guide to evaluating colocalization in biological microscopy. *Am J Physiol Cell Physiol* **300**, C723–C742 (2011).